



Updated search for B_c^+ decays to two charm mesons

LHCb collaboration[†]

Abstract

A data set corresponding to an integrated luminosity of 9 fb^{-1} of proton-proton collisions collected by the LHCb experiment has been analysed to search for $B_c^+ \rightarrow D_{(s)}^{(*)+} \bar{D}^{(*)0}$ decays. The decays are fully or partially reconstructed, where one or two missing neutral pions or photons from the decay of an excited charm meson are allowed. Upper limits for the branching fractions, normalised to B^+ decays to final states with similar topologies, are obtained for sixteen B_c^+ decay modes. For the decay $B_c^+ \rightarrow D_s^+ \bar{D}^0$, an excess with a significance of 3.4 standard deviations is found.

Published in JHEP 12 (2021) 117

© 2021 CERN for the benefit of the LHCb collaboration. CC BY 4.0 licence.

[†]Authors are listed at the end of this paper.

1 Introduction

Heavy-flavour states with b quarks are characterised by a relatively long lifetime and a large number of decay channels, and allow for highly sensitive studies of charge and parity (CP) symmetry violation and quantum-loop induced amplitudes. In the B_c^+ meson, a \bar{b} quark is accompanied by a charm quark, c , forming a system where decays of both the beauty and the charm quark, as well as weak annihilation processes, contribute to the decay amplitude [1].

Transition amplitudes between up-type quarks and down-type quarks are described by the Cabibbo-Kobayashi-Maskawa (CKM) quark-mixing matrix [2, 3]. Figure 1 illustrates the CKM-favoured, but colour-suppressed $B_c^+ \rightarrow D_s^+ \bar{D}^0$ decay (unless specified otherwise, charge conjugation is implied throughout this article) and the CKM-suppressed, but colour-favoured $B_c^+ \rightarrow D_s^+ D^0$ decay, which are expected to have similar amplitudes. This may result in a large, $\mathcal{O}(1)$, CP asymmetry for final states that are common between D^0 and \bar{D}^0 decays. Consequently decays of B_c^+ mesons to two charm mesons, $B_c^+ \rightarrow D_{(s)}^+ (\bar{D})^0$, have been proposed to measure the angle $\gamma \equiv \arg(-V_{ud}V_{ub}^*/V_{cd}V_{cb}^*)$ [4–7], one of the key parameters of the CKM matrix. Presently, the most precise determinations of γ come from measurements of the CP asymmetry in $B^+ \rightarrow (\bar{D})^0 K^+$ decays [8, 9].

Predicted branching fractions of B_c^+ decays to two charm mesons [10–14] are listed in Table 1. Final-state interactions may result in an enhancement of $B_c^+ \rightarrow D^+ (\bar{D})^0$ decay rates [15]. Moreover, contributions from physics beyond the Standard Model could potentially affect fully hadronic B decays [16–18].

This article describes a search for sixteen $B_c^+ \rightarrow D_{(s)}^{(*)+} (\bar{D})^{(*)0}$ decay channels, using proton-proton (pp) collision data collected by the LHCb experiment, corresponding to an integrated luminosity of 9 fb^{-1} , of which 1 fb^{-1} was recorded at a centre-of-mass energy $\sqrt{s} = 7 \text{ TeV}$, 2 fb^{-1} at $\sqrt{s} = 8 \text{ TeV}$ and 6 fb^{-1} at $\sqrt{s} = 13 \text{ TeV}$. The data taken at 7 and 8 TeV are referred to as Run 1, and the data taken at 13 TeV as Run 2. The Run 1 data has previously been analysed and no evidence of $B_c^+ \rightarrow D_{(s)}^{(*)+} (\bar{D})^{(*)0}$ decays was found [19].

Charm mesons are reconstructed in the $D^0 \rightarrow K^- \pi^+$, $D^0 \rightarrow K^- \pi^+ \pi^- \pi^+$, $D^+ \rightarrow K^- \pi^+ \pi^+$, $D_s^+ \rightarrow K^+ K^- \pi^+$, and $D^{*+} \rightarrow D^0 \pi^+$ decay modes. In the decay $B_c^+ \rightarrow D^{*+} (\bar{D})^0$, at least one of the neutral charm mesons is required to decay as $D^0 \rightarrow K^- \pi^+$. Partially reconstructed B_c^+ decays, which involve one or two excited charm mesons producing a photon or a neutral pion in their decay, are also included in the search.

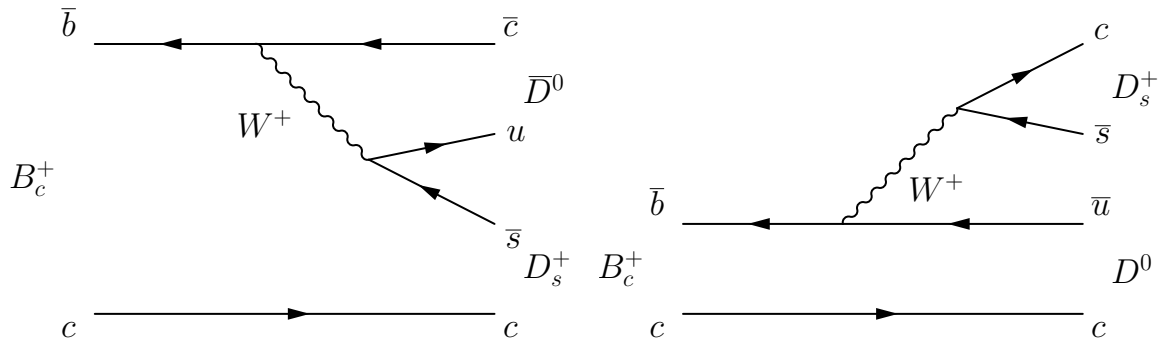


Figure 1: Diagrams for the (left) CKM-favoured, colour-suppressed $B_c^+ \rightarrow D_s^+ \bar{D}^0$ and (right) CKM-suppressed, colour-favoured $B_c^+ \rightarrow D_s^+ D^0$ decays.

Table 1: Predicted branching fractions of B_c^+ decays to two charm mesons, in units of 10^{-6} .

Channel	Ref. [11]	Ref. [12]	Ref. [13]	Ref. [14]
$B_c^+ \rightarrow D_s^+ \bar{D}^0$	2.3 ± 0.5	4.8	1.7	2.1
$B_c^+ \rightarrow D_s^+ D^0$	3.0 ± 0.5	6.6	2.5	7.4
$B_c^+ \rightarrow D^+ \bar{D}^0$	32 ± 7	53	32	33
$B_c^+ \rightarrow D^+ D^0$	0.10 ± 0.02	0.32	0.11	0.31
$B_c^+ \rightarrow D^{*+} \bar{D}^0$	12 ± 3	49	17	9
$B_c^+ \rightarrow D^{*+} D^0$	0.09 ± 0.02	0.40	0.38	0.44

These decays manifest themselves as relatively narrow structures in the mass distributions of the reconstructed final states below the B_c^+ mass.

The branching fractions, \mathcal{B} , of B_c^+ decays to fully reconstructed final states are measured relative to high-yield $B^+ \rightarrow D_{(s)}^{(*)+} \bar{D}^0$ normalisation modes,

$$R(D_{(s)}^{(*)+} \bar{D}^0) \equiv \frac{f_c \mathcal{B}(B_c^+ \rightarrow D_{(s)}^{(*)+} \bar{D}^0)}{f_u \mathcal{B}(B^+ \rightarrow D_{(s)}^{(*)+} \bar{D}^0)} = \frac{N(B_c^+ \rightarrow D_{(s)}^{(*)+} \bar{D}^0) \varepsilon(B^+ \rightarrow D_{(s)}^{(*)+} \bar{D}^0)}{\varepsilon(B_c^+ \rightarrow D_{(s)}^{(*)+} \bar{D}^0) N(B^+ \rightarrow D_{(s)}^{(*)+} \bar{D}^0)}, \quad (1)$$

where f_c/f_u is the ratio of the B_c^+ to B^+ fragmentation fraction, N denotes the measured $B_{(c)}^+$ yields, and ε represents the detection efficiencies. The value of $f_c/(f_u + f_d) \cdot \mathcal{B}(B_c^+ \rightarrow J/\psi \mu^+ \nu_\mu)$ has been measured at centre-of-mass energies of 7 and 13 TeV [20]. Under the assumption of equal production from hadronisation of B^+ and B^0 , $f_u = f_d$, the value of f_c/f_u is found to be 0.73% at $\sqrt{s} = 7$ TeV and 0.76% at $\sqrt{s} = 13$ TeV with relative uncertainties of approximately 25%, dominated by the uncertainty on the predicted value of $\mathcal{B}(B_c^+ \rightarrow J/\psi \mu^+ \nu_\mu)$, for which no measurements are available. Earlier measurements of f_c/f_u at 7 and 8 TeV using fully reconstructed B_c^+ decays found compatible values [21, 22].

The invariant-mass distributions of partially reconstructed $B_c^+ \rightarrow D_{(s)}^{*+} \bar{D}^0$ and $B_c^+ \rightarrow D_{(s)}^+ \bar{D}^{*0}$ decays overlap. Their branching fractions are measured separately by treating the contribution as arising entirely from each decay:

$$\begin{aligned} R'_+(D_{(s)}^+ \bar{D}^0) &\equiv \frac{f_c \mathcal{B}(B_c^+ \rightarrow D_{(s)}^{*+} \bar{D}^0)}{f_u \mathcal{B}(B^+ \rightarrow D_{(s)}^+ \bar{D}^0)} \\ &= \frac{N(B_c^+ \rightarrow D_{(s)}^{*+} \bar{D}^0) \varepsilon(B^+ \rightarrow D_{(s)}^+ \bar{D}^0)}{\varepsilon(B_c^+ \rightarrow D_{(s)}^{*+} \bar{D}^0) \mathcal{B}(D_{(s)}^{*+} \rightarrow D_{(s)}^+ X^0) N(B^+ \rightarrow D_{(s)}^+ \bar{D}^0)}, \end{aligned} \quad (2)$$

$$R'_0(D_{(s)}^+ \bar{D}^{*0}) \equiv \frac{f_c \mathcal{B}(B_c^+ \rightarrow D_{(s)}^+ \bar{D}^{*0})}{f_u \mathcal{B}(B^+ \rightarrow D_{(s)}^+ \bar{D}^0)} = \frac{N(B_c^+ \rightarrow D_{(s)}^+ \bar{D}^{*0}) \varepsilon(B^+ \rightarrow D_{(s)}^+ \bar{D}^0)}{\varepsilon(B_c^+ \rightarrow D_{(s)}^+ \bar{D}^{*0}) N(B^+ \rightarrow D_{(s)}^+ \bar{D}^0)}, \quad (3)$$

where X^0 represents a neutral pion or a photon. Decays of $B_c^+ \rightarrow D_{(s)}^{*+} \bar{D}^{*0}$ with a fully reconstructed $D^{*+} \rightarrow D^0 \pi^+$ decay, and one missing neutral pion or photon from the

\overline{D}^{*0} meson decay, results in measurements of

$$R'(D^{*+} \overline{D}^0) \equiv \frac{f_c \mathcal{B}(B_c^+ \rightarrow D^{*+} \overline{D}^{*0})}{f_u \mathcal{B}(B^+ \rightarrow D^{*+} \overline{D}^0)} = \frac{N(B_c^+ \rightarrow D^{*+} \overline{D}^{*0}) \varepsilon(B^+ \rightarrow D^{*+} \overline{D}^0)}{\varepsilon(B_c^+ \rightarrow D^{*+} \overline{D}^{*0}) N(B^+ \rightarrow D^{*+} \overline{D}^0)}. \quad (4)$$

The $B_c^+ \rightarrow D_s^{*+} \overline{D}^{*0}$ and $B_c^+ \rightarrow D^{*+} \overline{D}^{*0}$ decays can also be observed when both excited charm mesons decay with either a photon or a neutral pion and neither of the two neutral particles are reconstructed. In such cases, the ratio R'' is measured:

$$\begin{aligned} R''(D_{(s)}^+ \overline{D}^0) &\equiv \frac{f_c \mathcal{B}(B_c^+ \rightarrow D_{(s)}^{*+} \overline{D}^{*0})}{f_u \mathcal{B}(B^+ \rightarrow D_{(s)}^+ \overline{D}^0)} \\ &= \frac{N(B_c^+ \rightarrow D_{(s)}^{*+} \overline{D}^{*0}) \varepsilon(B^+ \rightarrow D_{(s)}^+ \overline{D}^0)}{\varepsilon(B_c^+ \rightarrow D_{(s)}^{*+} \overline{D}^{*0}) \mathcal{B}(D_{(s)}^{*+} \rightarrow D_{(s)}^+ X^0) N(B^+ \rightarrow D_{(s)}^+ \overline{D}^0)}. \end{aligned} \quad (5)$$

In total twenty ratios are measured, corresponding to sixteen B_c^+ branching fractions, since B_c^+ decays with a D^{*+} in the final state are searched for both in fully reconstructed $D^{*+} \rightarrow D^0 \pi^+$ and in partially reconstructed $D^{*+} \rightarrow D^+ X^0$ decays.

2 Detector and simulation

The LHCb detector [23, 24] is a single-arm forward spectrometer covering the pseudorapidity range $2 < \eta < 5$, designed for the study of particles containing b or c quarks. The detector includes a high-precision tracking system consisting of a silicon-strip vertex detector surrounding the pp interaction region [25], a large-area silicon-strip detector located upstream of a dipole magnet with a bending power of about 4 Tm, and three stations of silicon-strip detectors and straw drift tubes [26, 27] placed downstream of the magnet. The tracking system provides a measurement of the momentum, p , of charged particles with a relative uncertainty that varies from 0.5% at low momentum to 1.0% at 200 GeV/ c . The minimum distance of a track to a primary pp collision vertex (PV), the impact parameter, is measured with a resolution of $(15 + 29/p_T) \mu\text{m}$, where p_T is the component of the momentum transverse to the beam, in GeV/ c . Different types of charged hadrons are distinguished using information from two ring-imaging Cherenkov detectors [28]. Photons, electrons and hadrons are identified by a calorimeter system consisting of scintillating-pad and preshower detectors, an electromagnetic and a hadronic calorimeter. Muons are identified by a system composed of alternating layers of iron and multiwire proportional chambers [29]. The online event selection is performed by a trigger [30], which consists of a hardware stage, based on information from the calorimeter and muon systems, followed by a software stage, which applies a full event reconstruction.

At the hardware trigger stage, events are required to have a muon with high p_T or a hadron, photon or electron with high transverse energy in the calorimeters. For hadrons, the transverse energy threshold is 3.5 GeV. The software trigger requires a two-, three- or four-track secondary vertex with a significant displacement from any PV. At least one track should have $p_T > 1.7$ GeV/ c and χ_{IP}^2 with respect to any PV greater than 16, where χ_{IP}^2 is defined as the difference in the vertex-fit χ^2 of a given PV reconstructed with and without the considered particle. A multivariate algorithm [31, 32] is used for the identification of secondary vertices consistent with the decay of a b hadron.

Simulation is used to model the effects of the detector acceptance and the imposed selection requirements, as well as for the training of the multivariate selection of the B_c^+ signals, and for establishing the shape of the mass distributions of the signals. The PYTHIA [33] package, with a specific LHCb configuration [34], is used to simulate pp collisions with B^+ production. For B_c^+ production, the BCVEGPy [35] generator is used, interfaced with the Pythia parton shower and hadronisation model. Decays of unstable particles are described by EVTGEN [36], in which final-state radiation is generated using PHOTOS [37]. The interaction of the generated particles with the detector, and its response, are implemented using the GEANT4 toolkit [38] as described in Ref. [39]. The simulated B^+ production is corrected to match the observed spectrum of $B^+ \rightarrow D_s^+ \bar{D}^0$ decays in data, using a gradient boosted reweighter (GBR) [40] technique. The weights $w(p_T, y)$ are determined separately for Run 1 and Run 2. Simulated B_c^+ events are corrected to match the measured linear dependence of $f_c/(f_u + f_d)$ on p_T and y [20]. In addition, corrections using control samples are applied to the simulated events to improve the agreement with data regarding particle identification (PID) variables, the momentum scale and the momentum resolution.

3 Candidate selection

Charm-meson candidates are formed by combining two, three or four tracks that are incompatible with originating from any reconstructed PV. The tracks are required to form a high-quality vertex and the scalar sum of their p_T must exceed $1.8 \text{ GeV}/c$. To reduce background from misidentified particles, the pion and kaon candidates must also satisfy loose criteria on $DLL_{K\pi}$, the ratio of the likelihood between the kaon and pion PID hypotheses.

The reconstructed mass of D^0 , D_s^+ and D^+ candidates is required to be within $\pm 25 \text{ MeV}/c^2$ of their known values [41]. For channels with a fully reconstructed $D^{*+} \rightarrow D^0 \pi^+$ meson, the mass difference Δm between the D^{*+} and the D^0 candidates is required to be within $\pm 10 \text{ MeV}/c^2$ of the known value [41]. If more than one charm-meson candidate is formed from the same track combination, only the best according to PID information is selected.

A $B_{(c)}^+$ candidate is formed by combining a $D_{(s)}^{(*)+}$ candidate with a $(\bar{D})^0$ candidate if the combination has a p_T greater than $4.0 \text{ GeV}/c$, forms a good-quality vertex and originates from a PV. The reconstructed decay time of the charm meson candidates with respect to the $B_{(c)}^+$ vertex divided by its uncertainty, t/σ_t , is required to exceed -3 for D_s^+ and D^0 mesons. This requirement is increased to $+3$ for the longer-lived D^+ meson to eliminate background from $B^+ \rightarrow \bar{D}^0 \pi^+ \pi^- \pi^+$ decays where the negatively charged pion is misidentified as a kaon. Candidate B_c^+ decays that are compatible with the combination of a fully reconstructed $B_{(s)}^0 \rightarrow D_{(s)}^{(*)-} \pi^+ (\pi^- \pi^+)$ decay and a charged track are rejected. To eliminate duplicate tracks, the opening angles between any pair of final-state particles are required to be at least 0.5 mrad . The invariant-mass resolution of $B_{(c)}^+$ decays is significantly improved by applying a kinematic fit [42] where the invariant masses of the D^0 and the $D_{(s)}^{(*)+}$ candidates are constrained to their known values [41], all particles from the $D_{(s)}^{(*)+}$, D^0 , and $B_{(c)}^+$ decay are constrained to originate from their corresponding decay vertex and the $B_{(c)}^+$ candidate is constrained to originate from the PV with which it has

the smallest χ_{IP}^2 .

To reduce the combinatorial background, while maintaining high efficiency for signal, a multivariate selection based on a boosted decision tree (BDT) [43, 44] is employed. The BDT classifier exploits kinematic and PID properties of selected candidates, namely: the fit quality of the $B_{(c)}^+$ candidate and both charm-meson candidate vertices; the value of χ_{IP}^2 of the $B_{(c)}^+$ candidate; the values of t/σ_t of the $B_{(c)}^+$ and both charm-meson candidates; the reconstructed masses of the charm-meson candidates; and the reconstructed masses of the pairs of opposite-charge tracks from the $D_{(s)}^+$ candidate. In addition, for each charm-meson candidate, the smallest value of p_T and the smallest value of χ_{IP}^2 among the decay products, and the smallest (largest) value of $\text{DLL}_{K\pi}$ among all kaon (pion) candidates, are included as input variables for the BDT classifier.

The BDT training is performed separately for the $D_s^+ \bar{D}^0$, $D^+ \bar{D}^0$ and $D^{*+} \bar{D}^0$ final states, separately for the $D^0 \rightarrow K^- \pi^+$ and $D^0 \rightarrow K^- \pi^+ \pi^- \pi^+$ decay channels, and separately for the Run 1 and Run 2 data samples. For a given D^0 final state, the same classifier is used for both $B_c^+ \rightarrow D_{(s)}^{(*)+} \bar{D}^0$ and $B_c^+ \rightarrow D_{(s)}^{(*)+} D^0$ decays. For signal decays, the BDT classifier is trained using simulated B_c^+ events, while for background, data in the range $5350 < m(D_{(s)}^{(*)+} \bar{D}^0) < 6200 \text{ MeV}/c^2$ are used. For the background sample, the charm-meson mass windows are increased from $\pm 25 \text{ MeV}/c^2$ to $\pm 75 \text{ MeV}/c^2$, to increase the size of the training sample. The k -fold cross-training technique [45] with $k = 5$ is used to avoid biases in the calculation of the BDT output.

The data are divided in increasing order of signal purity into three samples having low, medium and high BDT output. Most of the sensitivity in this search comes from the data in the high BDT sample, but including data with lower signal purity increases the signal efficiency and constrains the shape of the combinatorial background. A small fraction of the events ($\approx 1\%$) have more than one $B_{(c)}^+$ candidate that satisfies the minimum BDT requirement. In such cases, one randomly selected candidate is retained per event. Figure 2 shows the invariant mass distributions of selected $B_{(c)}^+$ candidates in the highest BDT sample, summed over all D^0 final states.

4 Model of the $B_{(c)}^+$ mass distributions

To measure the signal yields, a model of the $B_{(c)}^+$ candidate mass distribution is fitted to the data in the range $5230 \leq m(D_{(s)}^{(*)+} \bar{D}^0) \leq 6700 \text{ MeV}/c^2$. The model consists of the following components, constrained to positive yields: the signals for fully reconstructed B^+ and B_c^+ decays; the signal for B_c^+ decays with one missing π^0 or photon; the signal for B_c^+ decays with two missing π^0 or photons; the background from $B^+ \rightarrow \bar{D}^0 K^+ K^- \pi^+$ decays; and the combinatorial background.

Fully reconstructed B^+ and B_c^+ signals are described by the sum of a Gaussian function and a Crystal Ball (CB) [46] function, extended to have power-law tails on both the low-mass and the high-mass sides. The CB and Gaussian components share a common peak position. The tail parameters of the CB and the ratio of the CB and Gaussian widths and integrals are determined from simulation, accounting for a dependence of both widths on the BDT output. The ratio of the B_c^+ and B^+ widths is determined from simulation, while the overall width of the B^+ is a free parameter in the fit to data, and is found to be consistent with the simulation. The peak position of the B^+ signal is a free parameter in

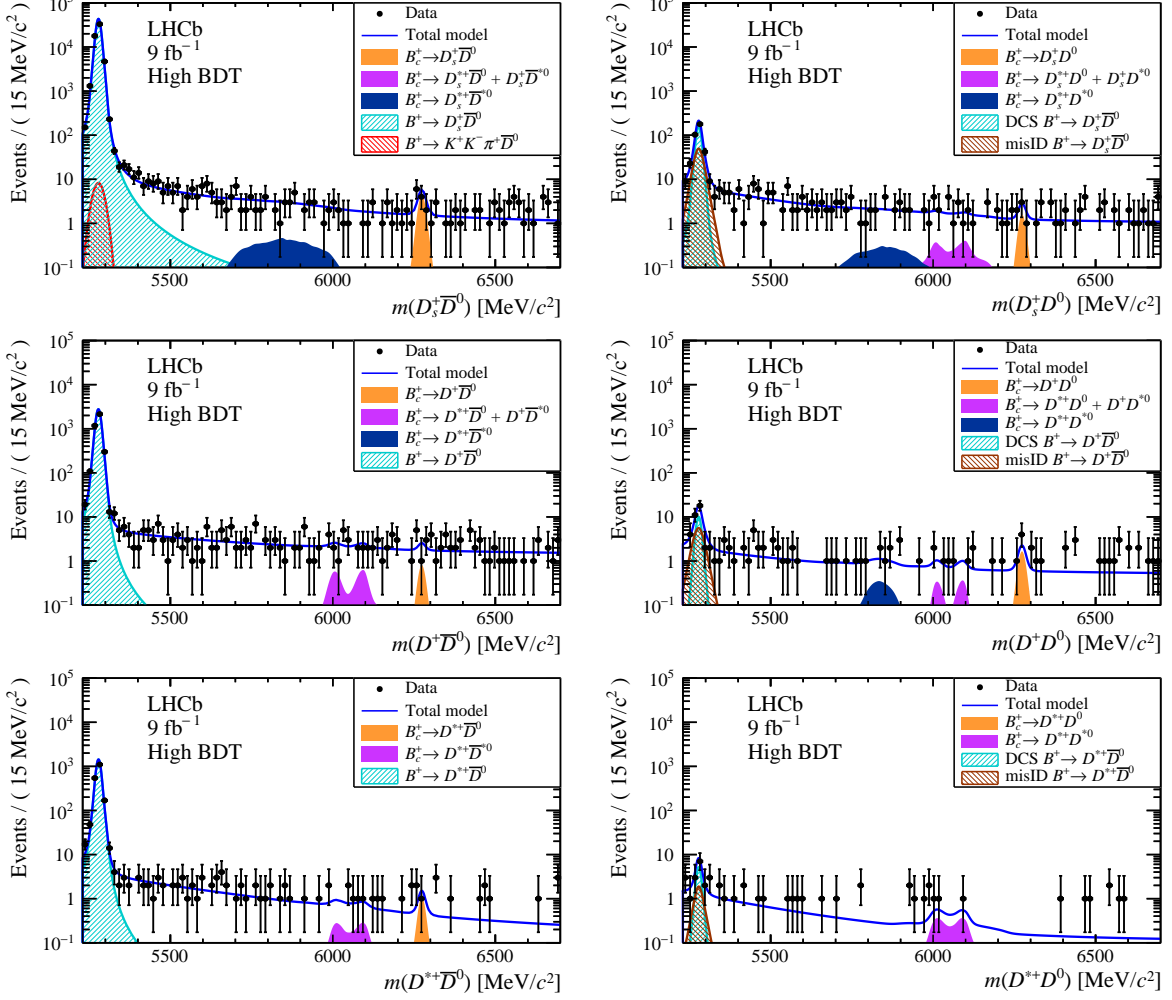


Figure 2: Invariant-mass distributions for the selected B_c^+ candidates in the highest BDT samples for (top left) $D_s^+ \bar{D}^0$, (top right) $D_s^+ D^0$, (center left) $D^+ \bar{D}^0$, (center right) $D^+ D^0$, (bottom left) $D^{*+} \bar{D}^0$ and (bottom right) $D^{*+} D^0$, final states. The overlaid curves correspond to the sum of the corresponding fit results.

the fit to data, and the known mass difference between the B^+ and the B_c^+ meson [41] is used to constrain the peak position of the B_c^+ signal.

Genuine $B^+ \rightarrow D_{(s)}^{(*)+} D^0$ decays are forbidden at tree level and consequently have a negligible yield, but doubly Cabibbo-suppressed (DCS) decays $\bar{D}^0 \rightarrow K^- \pi^+ (\pi^- \pi^+)$ result in crossfeed of $B^+ \rightarrow D_{(s)}^{(*)+} \bar{D}^0$ decays in the $D_{(s)}^{(*)+} D^0$ final state. An additional source of crossfeed into the $D_{(s)}^{(*)+} D^0$ final state is double misidentification of the pion and kaon in the Cabibbo-favoured $D^0 \rightarrow K^- \pi^+ (\pi^- \pi^+)$ decay. The DCS component is constrained in yield and shape by the large $B^+ \rightarrow D_{(s)}^{(*)+} \bar{D}^0$ signal, according to the known D^0 branching fractions [41]. For the shape of the misidentified component, the width of the $B^+ \rightarrow D_{(s)}^{(*)+} \bar{D}^0$ peak is scaled by a factor determined from a fit to $B^+ \rightarrow D_s^+ D^0$ candidates, and also used for the $B^+ \rightarrow D^{(*)+} D^0$ final states. The yield of the misidentified component is a free parameter in all fits to data.

Models for decays with one or two missing neutral particles from $D_{(s)}^{(*)+}$ and/or $D^{(*)0}$

decays are implemented as templates, obtained from kernel fits [47] to reconstructed mass distributions in simulation. Both longitudinal and transverse polarisations of $B_c^+ \rightarrow D_{(s)}^{*+} \bar{D}^{*0}$ decays contribute according to free polarisation fractions with different templates.

The Cabibbo-favoured $B^+ \rightarrow \bar{D}^0 K^+ K^- \pi^+$ decay is a background to the $B^+ \rightarrow D_s^+ \bar{D}^0$ channel, though its yield is strongly reduced by the D_s^+ mass requirement. This background is modelled by a single Gaussian function, with the width determined from a sample of simulated decays and the normalisation determined from the peak in the B^+ mass distribution in the D_s^+ invariant mass sideband.

The combinatorial background is described by the sum of an exponential function and a constant, where the parameters are allowed to differ between different D^0 decay modes, but are taken to be the same for all BDT samples of a given B_c^+ and D^0 decay channel. Studies of the charm-meson invariant-mass sidebands support these assumptions.

An unbinned extended maximum-likelihood fit is used to simultaneously describe the mass distributions of candidates in different BDT samples and different D^0 decay modes. In these fits the background and B^+ yields vary independently, but the branching fraction ratios R , $R'_{(+,0)}$ and R'' , defined in Eqs. 1–5, are constrained to be identical between the BDT samples and D^0 decay modes.

5 Systematic uncertainties

Systematic uncertainties that can be expressed as a relative uncertainty on the branching fraction ratio are evaluated separately for Run 1 and Run 2, and for each B_c^+ decay, D^0 channel and BDT sample. Their effective contributions in the fit, calculated as a weighted average over BDT samples and D^0 decay modes, are listed in Table 2. Where no uncertainty is given, this corresponds to either the absence of decays with two missing neutral particles in the $D^{*+} \bar{D}^0$ channel or the absence of the effect associated with an uncertainty in a given data-taking period or channel.

The uncertainty on the B_c^+ signal shape is evaluated by changing the B_c^+ signal shape to the sum of two Gaussian functions, and evaluating the median fractional change of the measured yield in pseudoexperiments performed with a background-only model. Uncertainties related to the B_c^+ production spectrum are evaluated by changing the slope parameters from Ref. [20] by their quoted uncertainties. The uncertainty on the p_T - and y -dependent weights used to correct the B^+ production spectrum in simulation is estimated by changing the settings of the GBR algorithm. Hit resolution parameterisation in the silicon vertex detector affects the χ_{IP}^2 distribution. The uncertainty associated with the parameterisation is therefore evaluated with simulation by varying the minimal value of the χ_{IP}^2 applied to the final-state tracks.

The limited size of the simulation samples results in uncertainties that are uncorrelated between the BDT samples and D^0 decay channels on the efficiency ratios $\varepsilon(B_c^+)/\varepsilon(B^+)$. All other systematic uncertainties are treated as fully correlated. A small uncertainty on the reconstruction efficiency results from that on the B_c^+ lifetime [41]. Uncertainties on the PID efficiencies cancel to first order in the ratio $\varepsilon(B_c^+)/\varepsilon(B^+)$ because of the identical particle content of the final state, and the difference in relative efficiencies with and without PID corrections is used to estimate the uncertainty from the PID correction procedure. The requirement to select at most one $B_{(c)}^+$ candidate per event introduces

Table 2: Effective contributions of the systematic uncertainties which are expressed as a relative uncertainty on the branching fraction ratio, combined over all BDT samples and D^0 decay modes, given in percent.

Final state	$D_s^+ \bar{D}^0$		$D^+ \bar{D}^0$		$D^{*+} \bar{D}^0$	
	Run 1	Run 2	Run 1	Run 2	Run 1	Run 2
B_c^+ signal shape	9.4	3.8	4.8	5.3	2.8	3.9
B_c^+ production spectrum	3.7	2.4	3.9	2.4	4.2	2.9
B^+ production spectrum	0.5	0.9	0.6	1.0	0.6	1.1
Hit resolution parameterisation	–	1.5	–	1.2	–	2.2
R simulation sample size	1.2	1.0	1.4	1.1	1.5	1.5
$R'_{(+,0)}$ simulation sample size	1.4	0.9	2.1	1.2	1.1	1.1
R'' simulation sample size	1.5	0.8	1.7	0.9	–	–
B_c^+ lifetime	1.3	1.4	1.3	1.3	2.1	2.6
PID efficiencies	1.6	1.2	2.8	0.8	2.2	1.4
Multiple $B_{(c)}^+$ candidates	0.4	0.4	0.6	0.5	1.4	1.2
Data-simulation differences	0.1	0.1	0.1	0.1	0.1	0.2
$B^+ \rightarrow \bar{D}^0 K^+ K^- \pi^+$	0.7	0.5	–	–	–	–
$\mathcal{B}(D^{*+} \rightarrow D^+ X^0)$	–	–	1.5	1.5	–	–
R total	10.4	5.3	7.2	6.6	6.3	6.5
$R'_{(+,0)}$ total	4.6	3.7	5.7	3.8	5.5	5.0
R'' total	4.6	3.7	5.5	3.7	–	–

an efficiency that may not be well reproduced by simulation. Therefore, the fraction of candidates removed by the requirement of at most one $B_{(c)}^+$ candidate per event is attributed as a systematic uncertainty. Residual differences appear in the comparison of the distributions of the BDT output between background-subtracted B^+ signal from data and simulation. The effect on the relative efficiency is evaluated by correcting the simulation to match the distributions in data. The background from $B^+ \rightarrow \bar{D}^0 K^+ K^- \pi^+$ decays to the $B^+ \rightarrow D_s^+ \bar{D}^0$ signal is assigned an uncertainty of 100% of its yield, resulting in a fractional uncertainty of less than 1%. The measurements of the branching fraction ratios according to Eqs. 2 and 5 involve the value of $\mathcal{B}(D^{*+} \rightarrow D^+ X^0)$, the uncertainty of which [41] is taken into account.

Other uncertainties, listed below, are instead taken into account by varying the fit model. Unless specified otherwise, these uncertainties are taken into account by replacing fixed values of the model parameters by their Gaussian constraints.

The uncertainty on the combinatorial background shape is evaluated by considering a single exponential function as an alternative to the exponential plus constant model, implemented using the discrete profiling method [48]. The B^+ shape uncertainty has a negligible effect on the B^+ yield but, because of its long tails, results in an uncertainty on the background shape. The effect is evaluated by assigning an uncertainty on the tail parameters determined from a fit to simulated events. The uncertainty on the α parameters of the CB function is increased by adding in quadrature the largest observed difference between data and simulation of this parameter in $B^+ \rightarrow D_s^+ \bar{D}^0$ decays.

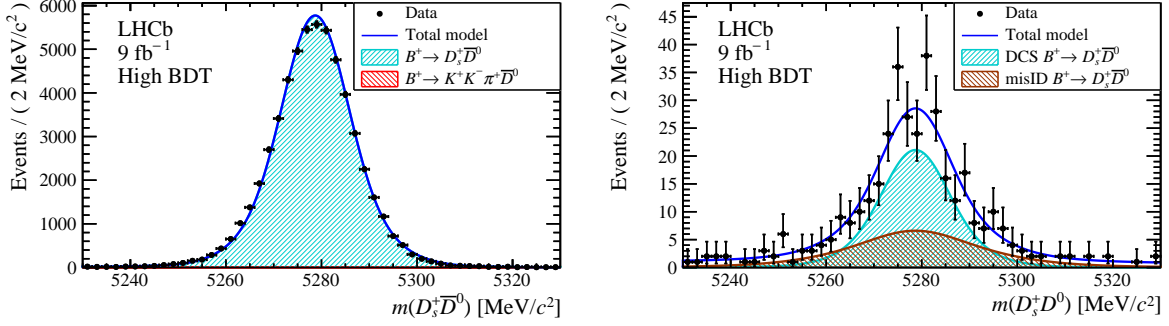


Figure 3: Invariant-mass distributions for the selected B^+ candidates in the highest BDT samples, in the region near the B^+ mass, for (left) $D_s^+ \bar{D}^0$ and (right) $D_s^+ D^0$ final states. The overlaid curves correspond to the sum of the corresponding fit results.

The fractional uncertainty on the yield of DCS crossfeed is the sum in quadrature of the fractional uncertainty on the normalisation yield and on the branching fractions $\mathcal{B}(D^0 \rightarrow K^+ \pi^- (\pi^+ \pi^-))$ [41]. The uncertainty on the difference between the B_c^+ and B^+ peak positions, $0.5 \text{ MeV}/c^2$, arises due to uncertainty on the measured masses [41, 49] and the momentum scale uncertainty [50]. The uncertainty on the ratio of the B_c^+ to B^+ invariant-mass resolution is determined from the statistical uncertainties of the fits to simulated decays. Statistical uncertainties in the templates of $B_c^+ \rightarrow D_{(s)}^{*+} (\bar{D})^0$ and $B_c^+ \rightarrow D_{(s)}^+ (\bar{D})^{*0}$ decays with one missing neutral pion or photon are accounted for by allowing a small contribution from the other template. The $B_c^+ \rightarrow D_{(s)}^{*+} (\bar{D})^{*0}$ signals have contributions from both transverse and longitudinal polarisations, which have differently shaped distributions of the reconstructed mass. This is accounted for by evaluating upper limits both for fully longitudinal and fully transverse polarisations, and reporting the least stringent upper limit. Including all model uncertainties results in an increase of the upper limits on the branching fraction ratios, discussed in Sec. 6, of 7% on average.

6 Results and conclusions

To determine the B_c^+ branching fraction ratios R , $R'_{(+,0)}$ and R'' , fits to data are performed separately for the six B_c^+ final states and for Run 1 and Run 2, while different D^0 decay modes and BDT samples are fit simultaneously. The results of the fits are shown in Fig. 2, where the data of the highest BDT samples and the corresponding fit results are summed over the D^0 decay channels and over data-taking periods. Detailed views of the $D_s^+ \bar{D}^0$ final states near the B^+ mass are shown in Fig. 3 which validate the model of the large $B^+ \rightarrow D_s^+ \bar{D}^0$ signal and its crossfeed to the $D_s^+ D^0$ final state. The integrals of the fit results in a $\pm 40 \text{ MeV}/c^2$ window around the B^+ mass differ less than 0.2% from the candidate counts.

The significance of the B_c^+ signals are calculated using Wilks' theorem [51] as $S = \sqrt{2\Delta \log \mathcal{L}}$, where $\Delta \log \mathcal{L}$ is the difference in the logarithm of the likelihood between the signal plus background and background-only hypotheses. Systematic uncertainties are included in the calculation of the significance through nuisance parameters in a minimised profile likelihood.

Evidence is found only for the decay $B_c^+ \rightarrow D_s^+ \bar{D}^0$ in Run 2 data, with a significance of 3.7 standard deviations, and the measured branching fraction ratio is $R(D_s^+ \bar{D}^0) = (3.6_{-1.2-0.2}^{+1.5+0.3}) \times 10^{-4}$, where the first uncertainty is statistical and the second is systematic. The quoted significance for this channel is compatible with estimates from simulated pseudoexperiments.

The values of R , $R'_{(+,0)}$ and R'' from Run 1 and Run 2 cannot be directly combined since the value of f_c/f_u depends on the pp centre-of-mass energy. Therefore, a combined fit of both the Run 1 and Run 2 data sets is made to the absolute B_c^+ branching fractions, using external input for $\mathcal{B}(B^+ \rightarrow D_s^+ \bar{D}^0)$, $\mathcal{B}(B^+ \rightarrow D^+ \bar{D}^0)$, $\mathcal{B}(B^+ \rightarrow D^{*+} \bar{D}^0)$ [41], and f_c/f_u [20], which depends on the theory prediction of $\mathcal{B}(B_c^+ \rightarrow J/\psi \mu^+ \nu_\mu)$. Corresponding uncertainties are included. In this combined fit the excess for $B_c^+ \rightarrow D_s^+ \bar{D}^0$ has a significance of 3.4 standard deviations, or 2.5 standard deviations when considering the probability of the excess to appear in any of the sixteen final states considered. The corresponding value of the branching fraction is $\mathcal{B}(B_c^+ \rightarrow D_s^+ \bar{D}^0) = (3.5_{-1.3-0.2}^{+1.5+0.3} \pm 1.0) \times 10^{-4}$, where the first uncertainty is statistical, the second systematic and the third due to external input.

Upper limits are reported on the ratio of branching fractions for all decays, calculated at 90% and 95% confidence level (C.L.) with the frequentist CL_s method [52,53], separately for Run 1 and Run 2. These limits are listed in Table 3. Limits for Run 1 are tighter than in Ref. [19] in particular for $R'_{(+,0)}$ and R'' , mainly because of better constraints on the shape of the combinatorial background.

Upper limits on the absolute B_c^+ branching fractions are based on the Run 2 dataset alone, which has nearly four times the sensitivity of the Run 1 dataset. The upper limits at 90(95%) C.L. are

$$\begin{aligned}
\mathcal{B}(B_c^+ \rightarrow D_s^+ \bar{D}^0) &< 7.2 (8.4) \times 10^{-4}; \\
\mathcal{B}(B_c^+ \rightarrow D_s^+ D^0) &< 3.0 (3.7) \times 10^{-4}; \\
\mathcal{B}(B_c^+ \rightarrow D^+ \bar{D}^0) &< 1.9 (2.5) \times 10^{-4}; \\
\mathcal{B}(B_c^+ \rightarrow D^+ D^0) &< 1.4 (1.8) \times 10^{-4}; \\
\mathcal{B}(B_c^+ \rightarrow D_s^{*+} \bar{D}^0) &< 5.3 (5.7) \times 10^{-4}; \\
\mathcal{B}(B_c^+ \rightarrow D_s^+ \bar{D}^{*0}) &< 4.6 (5.6) \times 10^{-4}; \\
\mathcal{B}(B_c^+ \rightarrow D_s^{*+} D^0) &< 0.9 (1.0) \times 10^{-3}; \\
\mathcal{B}(B_c^+ \rightarrow D_s^+ D^{*0}) &< 6.6 (8.4) \times 10^{-4}; \\
\mathcal{B}(B_c^+ \rightarrow D^{*+} \bar{D}^0) &< 3.8 (4.8) \times 10^{-4}; \\
\mathcal{B}(B_c^+ \rightarrow D^{*+} D^0) &< 2.0 (2.4) \times 10^{-4}; \\
\mathcal{B}(B_c^+ \rightarrow D^+ \bar{D}^{*0}) &< 6.5 (8.2) \times 10^{-4}; \\
\mathcal{B}(B_c^+ \rightarrow D^+ D^{*0}) &< 3.7 (4.6) \times 10^{-4}; \\
\mathcal{B}(B_c^+ \rightarrow D_s^{*+} \bar{D}^{*0}) &< 1.3 (1.5) \times 10^{-3}; \\
\mathcal{B}(B_c^+ \rightarrow D_s^{*+} D^{*0}) &< 1.3 (1.6) \times 10^{-3}; \\
\mathcal{B}(B_c^+ \rightarrow D^{*+} \bar{D}^{*0}) &< 1.0 (1.3) \times 10^{-3}; \\
\mathcal{B}(B_c^+ \rightarrow D^{*+} D^{*0}) &< 7.7 (8.9) \times 10^{-4}.
\end{aligned}$$

The reported upper limits on B_c^+ decays with a D^{*+} meson in the final state are based on the analyses of fully reconstructed $D^{*+} \rightarrow D^0 \pi^+$ decays, which have a higher sensitivity

Table 3: Upper limits on the branching fraction ratios R , $R'_{(+,0)}$ and R'' of B_c^+ to B^+ decays, defined in Eqs. 1–5, at the 90(95)% C.L. for Run 2 and Run 1 data, in units of 10^{-3} .

	Run 2 6 fb $^{-1}$, 13 TeV	Run 1 3 fb $^{-1}$, 7 and 8 TeV
$R(D_s^+ \bar{D}^0)$	0.57 (0.62)	0.45 (0.58)
$R'_+(D_s^+ \bar{D}^0)$	0.36 (0.42)	0.45 (0.75)
$R'_0(D_s^+ \bar{D}^0)$	0.27 (0.36)	0.64 (0.71)
$R''(D_s^+ \bar{D}^0)$	0.9 (1.1)	1.1 (1.5)
$R(D_s^+ D^0)$	0.22 (0.25)	0.51 (0.62)
$R'_+(D_s^+ D^0)$	0.59 (0.72)	0.76 (0.89)
$R'_0(D_s^+ D^0)$	0.49 (0.60)	0.74 (0.88)
$R''(D_s^+ D^0)$	0.9 (1.0)	1.6 (2.3)
$R(D^+ \bar{D}^0)$	3.5 (4.4)	8 (11)
$R'_+(D^+ \bar{D}^0)$	26 (33)	45 (52)
$R'_0(D^+ \bar{D}^0)$	11 (12)	16 (20)
$R''(D^+ \bar{D}^0)$	21 (28)	90 (110)
$R(D^+ D^0)$	2.9 (3.6)	12 (14)
$R'_+(D^+ D^0)$	18 (21)	17 (33)
$R'_0(D^+ D^0)$	6.6 (7.3)	8.2 (9.8)
$R''(D^+ D^0)$	17 (20)	82 (94)
$R(D^{*+} \bar{D}^0)$	6.9 (8.4)	26 (28)
$R'(D^{*+} \bar{D}^0)$	16 (19)	31 (44)
$R(D^{*+} D^0)$	3.6 (4.4)	8 (13)
$R'(D^{*+} D^0)$	12 (15)	36 (45)

than the channels with partially reconstructed $D^{*+} \rightarrow D^+ X^0$ decays.

In conclusion, this article reports the results of a search for $B_c^+ \rightarrow D_{(s)}^{(*)+} \bar{D}^0$ decays, covering sixteen B_c^+ decay channels, which include partially reconstructed decays where one or two neutral pions or photons from the decay of an excited charm meson are not reconstructed. The results, based on pp collision data corresponding to 9 fb^{-1} of integrated luminosity, supersede an earlier LHCb measurement [19] on Run 1 data only. No signal is observed in any of the channels investigated, consistent with the Standard Model expectation. An excess with a significance of 3.4 standard deviations is found for the decay $B_c^+ \rightarrow D_s^+ \bar{D}^0$, which is in tension with the theoretical expectation [11–14].

Acknowledgements

We express our gratitude to our colleagues in the CERN accelerator departments for the excellent performance of the LHC. We thank the technical and administrative staff at the LHCb institutes. We acknowledge support from CERN and from the national agencies: CAPES, CNPq, FAPERJ and FINEP (Brazil); MOST and NSFC (China); CNRS/IN2P3 (France); BMBF, DFG and MPG (Germany); INFN (Italy); NWO (Netherlands); MNiSW

and NCN (Poland); MEN/IFA (Romania); MSHE (Russia); MICINN (Spain); SNSF and SER (Switzerland); NASU (Ukraine); STFC (United Kingdom); DOE NP and NSF (USA). We acknowledge the computing resources that are provided by CERN, IN2P3 (France), KIT and DESY (Germany), INFN (Italy), SURF (Netherlands), PIC (Spain), GridPP (United Kingdom), RRCKI and Yandex LLC (Russia), CSCS (Switzerland), IFIN-HH (Romania), CBPF (Brazil), PL-GRID (Poland) and NERSC (USA). We are indebted to the communities behind the multiple open-source software packages on which we depend. Individual groups or members have received support from ARC and ARDC (Australia); AvH Foundation (Germany); EPLANET, Marie Skłodowska-Curie Actions and ERC (European Union); A*MIDEX, ANR, IPhU and Labex P2IO, and Région Auvergne-Rhône-Alpes (France); Key Research Program of Frontier Sciences of CAS, CAS PIFI, CAS CCEPP, Fundamental Research Funds for the Central Universities, and Sci. & Tech. Program of Guangzhou (China); RFBR, RSF and Yandex LLC (Russia); GVA, XuntaGal and GENCAT (Spain); the Leverhulme Trust, the Royal Society and UKRI (United Kingdom).

References

- [1] LHCb collaboration, R. Aaij *et al.*, *Observation of $B_c^+ \rightarrow D^0 K^+$ decays*, Phys. Rev. Lett. **118** (2017) 111803, [arXiv:1701.01856](#).
- [2] N. Cabibbo, *Unitary symmetry and leptonic decays*, Phys. Rev. Lett. **10** (1963) 531.
- [3] M. Kobayashi and T. Maskawa, *CP-violation in the renormalizable theory of weak interaction*, Prog. Theor. Phys. **49** (1973) 652.
- [4] M. Masetti, *CP violation in B_c^+ decays*, Phys. Lett. **B286** (1992) 160.
- [5] R. Fleischer and D. Wyler, *Exploring CP violation with B_c^+ decays*, Phys. Rev. **D62** (2000) 057503, [arXiv:hep-ph/0004010](#).
- [6] A. K. Giri, R. Mohanta, and M. P. Khanna, *Determination of the angle γ from nonleptonic $B_c^+ \rightarrow D_s^+ D^0$ decays*, Phys. Rev. **D65** (2002) 034016, [arXiv:hep-ph/0104009](#).
- [7] A. K. Giri, B. Mawlong, and R. Mohanta, *Determining the CKM angle γ with B_c^+ decays*, Phys. Rev. **D75** (2007) 097304, [arXiv:hep-ph/0611212](#), [Erratum: Phys. Rev. **D76**, 099902(2007)].
- [8] LHCb collaboration, R. Aaij *et al.*, *Measurement of CP observables in $B^\pm \rightarrow D^{(*)} K^\pm$ and $B^\pm \rightarrow D^{(*)} \pi^\pm$ decays using two-body D final states*, JHEP **04** (2021) 081, [arXiv:2012.09903](#).
- [9] LHCb collaboration, R. Aaij *et al.*, *Measurement of the CKM angle γ in $B^\pm \rightarrow DK^\pm$ and $B^\pm \rightarrow D\pi^\pm$ decays with $D \rightarrow K_S h^+ h^-$* , JHEP **02** (2021) 0169, [arXiv:2010.08483](#).
- [10] A. Abd El-Hady, J. H. Munoz, and J. P. Vary, *Semileptonic and nonleptonic B_c decays*, Phys. Rev. D **62** (2000) 014019, [arXiv:hep-ph/9909406](#).
- [11] Z. Rui, Z. Zhitian, and C.-D. Lu, *The double charm decays of B_c meson in the perturbative QCD approach*, Phys. Rev. **D86** (2012) 074019, [arXiv:1203.2303](#).
- [12] V. V. Kiselev, *Gold plated mode of CP violation in decays of B_c meson from QCD sum rules*, J. Phys. G **30** (2004) 1445, [arXiv:hep-ph/0302241](#).
- [13] M. A. Ivanov, J. G. Korner, and O. N. Pakhomova, *The nonleptonic decays $B_c^+ \rightarrow D_s^+ \bar{D}^0$ and $B_c^+ \rightarrow D_s^+ D^0$ in a relativistic quark model*, Phys. Lett. **B555** (2003) 189, [arXiv:hep-ph/0212291](#).
- [14] M. A. Ivanov, J. G. Korner, and P. Santorelli, *Exclusive semileptonic and nonleptonic decays of the B_c meson*, Phys. Rev. **D73** (2006) 054024, [arXiv:hep-ph/0602050](#).
- [15] B. Mohammadi, *Final state interaction analysis and branching fraction calculations of $B_c^+ \rightarrow D^+ \bar{D}^0 (D^+ D^0)$ decays*, Few Body Syst. **62** (2021) 19.
- [16] M. Bordone *et al.*, *A puzzle in $\bar{B}_{(s)}^0 \rightarrow D_{(s)}^{(*)+} \{\pi^-, K^-\}$ decays and extraction of the f_s/f_d fragmentation fraction*, Eur. Phys. J. **C80** (2020) 951, [arXiv:2007.10338](#).

- [17] S. Iguro and T. Kitahara, *Implications for new physics from a novel puzzle in $\bar{B}_{(s)}^0 \rightarrow D_{(s)}^{(*)+} \{\pi^-, K^-\}$ decays*, Phys. Rev. **D102** (2020) 071701, arXiv:2008.01086.
- [18] F.-M. Cai, W.-J. Deng, X.-Q. Li, and Y.-D. Yang, *Probing new physics in class-I B-meson decays into heavy-light final states*, arXiv:2103.04138.
- [19] LHCb collaboration, R. Aaij *et al.*, *Search for B_c^+ decays to two charm mesons*, Nucl. Phys. **B930** (2018) 563, arXiv:1712.04702.
- [20] LHCb collaboration, R. Aaij *et al.*, *Measurement of the B_c^- production fraction and asymmetry in 7 and 13 TeV pp collisions*, Phys. Rev. **D100** (2019) 112006, arXiv:1910.13404.
- [21] LHCb collaboration, R. Aaij *et al.*, *Measurements of B_c^+ production and mass with the $B_c^+ \rightarrow J/\psi\pi^+$ decay*, Phys. Rev. Lett. **109** (2012) 232001, arXiv:1209.5634.
- [22] LHCb collaboration, R. Aaij *et al.*, *Measurement of B_c^+ production in proton-proton collisions at $\sqrt{s} = 8$ TeV*, Phys. Rev. Lett. **114** (2015) 132001, arXiv:1411.2943.
- [23] LHCb collaboration, A. A. Alves Jr. *et al.*, *The LHCb detector at the LHC*, JINST **3** (2008) S08005.
- [24] LHCb collaboration, R. Aaij *et al.*, *LHCb detector performance*, Int. J. Mod. Phys. **A30** (2015) 1530022, arXiv:1412.6352.
- [25] R. Aaij *et al.*, *Performance of the LHCb Vertex Locator*, JINST **9** (2014) P09007, arXiv:1405.7808.
- [26] R. Arink *et al.*, *Performance of the LHCb Outer Tracker*, JINST **9** (2014) P01002, arXiv:1311.3893.
- [27] P. d'Argent *et al.*, *Improved performance of the LHCb Outer Tracker in LHC Run 2*, JINST **12** (2017) P11016, arXiv:1708.00819.
- [28] M. Adinolfi *et al.*, *Performance of the LHCb RICH detector at the LHC*, Eur. Phys. J. **C73** (2013) 2431, arXiv:1211.6759.
- [29] A. A. Alves Jr. *et al.*, *Performance of the LHCb muon system*, JINST **8** (2013) P02022, arXiv:1211.1346.
- [30] R. Aaij *et al.*, *The LHCb trigger and its performance in 2011*, JINST **8** (2013) P04022, arXiv:1211.3055.
- [31] V. V. Gligorov and M. Williams, *Efficient, reliable and fast high-level triggering using a bonsai boosted decision tree*, JINST **8** (2013) P02013, arXiv:1210.6861.
- [32] T. Likhomanenko *et al.*, *LHCb topological trigger reoptimization*, J. Phys. Conf. Ser. **664** (2015) 082025.
- [33] T. Sjöstrand, S. Mrenna, and P. Skands, *A brief introduction to PYTHIA 8.1*, Comput. Phys. Commun. **178** (2008) 852, arXiv:0710.3820; T. Sjöstrand, S. Mrenna, and P. Skands, *PYTHIA 6.4 physics and manual*, JHEP **05** (2006) 026, arXiv:hep-ph/0603175.

- [34] I. Belyaev *et al.*, *Handling of the generation of primary events in Gauss, the LHCb simulation framework*, J. Phys. Conf. Ser. **331** (2011) 032047.
- [35] C.-H. Chang, C. Driouichi, P. Eerola, and X. G. Wu, *BCVEGPY: An event generator for hadronic production of the B_c meson*, Comput. Phys. Commun. **159** (2004) 192, arXiv:hep-ph/0309120.
- [36] D. J. Lange, *The EvtGen particle decay simulation package*, Nucl. Instrum. Meth. **A462** (2001) 152.
- [37] N. Davidson, T. Przedzinski, and Z. Was, *PHOTOS interface in C++: Technical and physics documentation*, Comp. Phys. Comm. **199** (2016) 86, arXiv:1011.0937.
- [38] Geant4 collaboration, J. Allison *et al.*, *Geant4 developments and applications*, IEEE Trans. Nucl. Sci. **53** (2006) 270; Geant4 collaboration, S. Agostinelli *et al.*, *Geant4: A simulation toolkit*, Nucl. Instrum. Meth. **A506** (2003) 250.
- [39] M. Clemencic *et al.*, *The LHCb simulation application, Gauss: Design, evolution and experience*, J. Phys. Conf. Ser. **331** (2011) 032023.
- [40] A. Rogozhnikov, *Reweighting with Boosted Decision Trees*, J. Phys. Conf. Ser. **762** (2016) 012036, arXiv:1608.05806, https://github.com/arogozhnikov/hep_ml.
- [41] Particle Data Group, P. A. Zyla *et al.*, *Review of particle physics*, Prog. Theor. Exp. Phys. **2020** (2020) 083C01.
- [42] W. D. Hulsbergen, *Decay chain fitting with a Kalman filter*, Nucl. Instrum. Meth. **A552** (2005) 566, arXiv:physics/0503191.
- [43] L. Breiman, J. H. Friedman, R. A. Olshen, and C. J. Stone, *Classification and regression trees*, Wadsworth international group, Belmont, California, USA, 1984.
- [44] B. P. Roe *et al.*, *Boosted decision trees as an alternative to artificial neural networks for particle identification*, Nucl. Instrum. Meth. **A543** (2005) 577, arXiv:physics/0408124.
- [45] S. Geisser, *Predictive inference: An introduction*, Monographs on statistics and applied probability, Chapman & Hall, New York, 1993.
- [46] T. Skwarnicki, *A study of the radiative cascade transitions between the Upsilon-prime and Upsilon resonances*, PhD thesis, Institute of Nuclear Physics, Krakow, 1986, DESY-F31-86-02.
- [47] K. Cranmer, *Kernel estimation in high-energy physics*, Computer Physics Communications **136** (2001) 198, arXiv:hep-ex/0011057.
- [48] P. D. Dauncey, M. Kenzie, N. Wardle, and G. J. Davies, *Handling uncertainties in background shapes: the discrete profiling method*, JINST **10** (2015) P04015, arXiv:1408.6865.
- [49] LHCb collaboration, R. Aaij *et al.*, *Precision measurement of the B_c^+ meson mass*, JHEP **07** (2020) 123, arXiv:2004.08163.

- [50] LHCb collaboration, R. Aaij *et al.*, *Measurements of the Λ_b^0 , Ξ_b^- , and Ω_b^- baryon masses*, Phys. Rev. Lett. **110** (2013) 182001, [arXiv:1302.1072](#).
- [51] S. S. Wilks, *The large-sample distribution of the likelihood ratio for testing composite hypotheses*, Ann. Math. Stat. **9** (1938) 60.
- [52] A. L. Read, *Presentation of search results: the CL_s technique*, Journal of Physics G: Nuclear and Particle Physics **28** (2002) 2693.
- [53] M. Kenzie *et al.*, *GammaCombo: A statistical analysis framework for combining measurements, fitting datasets and producing confidence intervals*, doi: 10.5281/zenodo.3371421.

LHCb collaboration

R. Aaij³², A.S.W. Abdelmotteleb⁵⁶, C. Abellán Beteta⁵⁰, T. Ackernley⁶⁰, B. Adeva⁴⁶, M. Adinolfi⁵⁴, H. Afsharnia⁹, C. Agapopoulou¹³, C.A. Aidala⁸⁶, S. Aiola²⁵, Z. Ajaltouni⁹, S. Akar⁶⁵, J. Albrecht¹⁵, F. Alessio⁴⁸, M. Alexander⁵⁹, A. Alfonso Alberio⁴⁵, Z. Aliouche⁶², G. Alkhazov³⁸, P. Alvarez Cartelle⁵⁵, S. Amato², J.L. Amey⁵⁴, Y. Amhis¹¹, L. An⁴⁸, L. Anderlini²², A. Andreianov³⁸, M. Andreotti²¹, F. Archilli¹⁷, A. Artamonov⁴⁴, M. Artuso⁶⁸, K. Arzymatov⁴², E. Aslanides¹⁰, M. Atzeni⁵⁰, B. Audurier¹², S. Bachmann¹⁷, M. Bachmayer⁴⁹, J.J. Back⁵⁶, P. Baladron Rodriguez⁴⁶, V. Balagura¹², W. Baldini²¹, J. Baptista Leite¹, M. Barbetti²², R.J. Barlow⁶², S. Barsuk¹¹, W. Barter⁶¹, M. Bartolini^{24,h}, F. Baryshnikov⁸³, J.M. Basels¹⁴, S. Bashir³⁴, G. Bassi²⁹, B. Batsukh⁶⁸, A. Battig¹⁵, A. Bay⁴⁹, A. Beck⁵⁶, M. Becker¹⁵, F. Bedeschi²⁹, I. Bediaga¹, A. Beiter⁶⁸, V. Belavin⁴², S. Belin²⁷, V. Bellee⁵⁰, K. Belous⁴⁴, I. Belov⁴⁰, I. Belyaev⁴¹, G. Bencivenni²³, E. Ben-Haim¹³, A. Berezhnoy⁴⁰, R. Bernet⁵⁰, D. Berninghoff¹⁷, H.C. Bernstein⁶⁸, C. Bertella⁴⁸, A. Bertolin²⁸, C. Betancourt⁵⁰, F. Betti⁴⁸, I.A. Bezshyiko⁵⁰, S. Bhasin⁵⁴, J. Bhom³⁵, L. Bian⁷³, M.S. Bieker¹⁵, S. Bifani⁵³, P. Billoir¹³, M. Birch⁶¹, F.C.R. Bishop⁵⁵, A. Bitadze⁶², A. Bizzeti^{22,k}, M. Bjørn⁶³, M.P. Blago⁴⁸, T. Blake⁵⁶, F. Blanc⁴⁹, S. Blusk⁶⁸, D. Bobulska⁵⁹, J.A. Boelhauve¹⁵, O. Boente Garcia⁴⁶, T. Boettcher⁶⁵, A. Boldyrev⁸², A. Bondar⁴³, N. Bondar^{38,48}, S. Borghi⁶², M. Borisyak⁴², M. Borsato¹⁷, J.T. Borsuk³⁵, S.A. Bouchiba⁴⁹, T.J.V. Bowcock⁶⁰, A. Boyer⁴⁸, C. Bozzi²¹, M.J. Bradley⁶¹, S. Braun⁶⁶, A. Brea Rodriguez⁴⁶, M. Brodski⁴⁸, J. Brodzicka³⁵, A. Brossa Gonzalo⁵⁶, D. Brundu²⁷, A. Buonauro⁵⁰, L. Buonincontri²⁸, A.T. Burke⁶², C. Burr⁴⁸, A. Bursche⁷², A. Butkevich³⁹, J.S. Butter³², J. Buytaert⁴⁸, W. Byczynski⁴⁸, S. Cadeddu²⁷, H. Cai⁷³, R. Calabrese^{21,f}, L. Calefice^{15,13}, L. Calero Diaz²³, S. Cali²³, R. Calladine⁵³, M. Calvi^{26,j}, M. Calvo Gomez⁸⁵, P. Camargo Magalhaes⁵⁴, P. Campana²³, A.F. Campoverde Quezada⁶, S. Capelli^{26,j}, L. Capriotti^{20,d}, A. Carbone^{20,d}, G. Carboni³¹, R. Cardinale^{24,h}, A. Cardini²⁷, I. Carli⁴, P. Carniti^{26,j}, L. Carus¹⁴, K. Carvalho Akiba³², A. Casais Vidal⁴⁶, G. Casse⁶⁰, M. Cattaneo⁴⁸, G. Cavallero⁴⁸, S. Celani⁴⁹, J. Cerasoli¹⁰, D. Cervenkov⁶³, A.J. Chadwick⁶⁰, M.G. Chapman⁵⁴, M. Charles¹³, Ph. Charpentier⁴⁸, G. Chatzikonstantinidis⁵³, C.A. Chavez Barajas⁶⁰, M. Chefdeville⁸, C. Chen³, S. Chen⁴, A. Chernov³⁵, V. Chobanova⁴⁶, S. Cholak⁴⁹, M. Chruszcz³⁵, A. Chubykin³⁸, V. Chulikov³⁸, P. Ciambone²³, M.F. Cicala⁵⁶, X. Cid Vidal⁴⁶, G. Ciezarek⁴⁸, P.E.L. Clarke⁵⁸, M. Clemencic⁴⁸, H.V. Cliff⁵⁵, J. Closier⁴⁸, J.L. Cobbledick⁶², V. Coco⁴⁸, J.A.B. Coelho¹¹, J. Cogan¹⁰, E. Cogneras⁹, L. Cojocariu³⁷, P. Collins⁴⁸, T. Colombo⁴⁸, L. Congedo^{19,c}, A. Contu²⁷, N. Cooke⁵³, G. Coombs⁵⁹, I. Corredoira⁴⁶, G. Corti⁴⁸, C.M. Costa Sobral⁵⁶, B. Couturier⁴⁸, D.C. Craik⁶⁴, J. Crkovská⁶⁷, M. Cruz Torres¹, R. Currie⁵⁸, C.L. Da Silva⁶⁷, S. Dadabaev⁸³, L. Dai⁷¹, E. Dall'Occo¹⁵, J. Dalseno⁴⁶, C. D'Ambrosio⁴⁸, A. Danilina⁴¹, P. d'Argent⁴⁸, J.E. Davies⁶², A. Davis⁶², O. De Aguiar Francisco⁶², K. De Bruyn⁷⁹, S. De Capua⁶², M. De Cian⁴⁹, J.M. De Miranda¹, L. De Paula², M. De Serio^{19,c}, D. De Simone⁵⁰, P. De Simone²³, J.A. de Vries⁸⁰, C.T. Dean⁶⁷, D. Decamp⁸, V. Dedu¹⁰, L. Del Buono¹³, B. Delaney⁵⁵, H.-P. Dembinski¹⁵, A. Dendek³⁴, V. Denysenko⁵⁰, D. Derkach⁸², O. Deschamps⁹, F. Desse¹¹, F. Dettori^{27,e}, B. Dey⁷⁷, A. Di Cicco²³, P. Di Nezza²³, S. Didenko⁸³, L. Dieste Maronas⁴⁶, H. Dijkstra⁴⁸, V. Dobishuk⁵², C. Dong³, A.M. Donohoe¹⁸, F. Dordei²⁷, A.C. dos Reis¹, L. Douglas⁵⁹, A. Dovbnya⁵¹, A.G. Downes⁸, M.W. Dudek³⁵, L. Dufour⁴⁸, V. Duk⁷⁸, P. Durante⁴⁸, J.M. Durham⁶⁷, D. Dutta⁶², A. Dziurda³⁵, A. Dzyuba³⁸, S. Easo⁵⁷, U. Egede⁶⁹, V. Egorychev⁴¹, S. Eidelman^{43,v}, S. Eisenhardt⁵⁸, S. Ek-In⁴⁹, L. Eklund^{59,w}, S. Ely⁶⁸, A. Ene³⁷, E. Epple⁶⁷, S. Escher¹⁴, J. Eschle⁵⁰, S. Esen¹³, T. Evans⁴⁸, A. Falabella²⁰, J. Fan³, Y. Fan⁶, B. Fang⁷³, S. Farry⁶⁰, D. Fazzini^{26,j}, M. Féo⁴⁸, A. Fernandez Prieto⁴⁶, A.D. Fernandez⁶⁶, F. Ferrari^{20,d}, L. Ferreira Lopes⁴⁹, F. Ferreira Rodrigues², S. Ferreres Sole³², M. Ferrillo⁵⁰, M. Ferro-Luzzi⁴⁸, S. Filippov³⁹, R.A. Fini¹⁹, M. Fiorini^{21,f}, M. Firlej³⁴, K.M. Fischer⁶³, D.S. Fitzgerald⁸⁶, C. Fitzpatrick⁶², T. Fiutowski³⁴, A. Fkiaras⁴⁸, F. Fleuret¹²,

M. Fontana¹³, F. Fontanelli^{24,h}, R. Forty⁴⁸, D. Foulds-Holt⁵⁵, V. Franco Lima⁶⁰,
M. Franco Sevilla⁶⁶, M. Frank⁴⁸, E. Franzoso²¹, G. Frau¹⁷, C. Frei⁴⁸, D.A. Friday⁵⁹, J. Fu²⁵,
Q. Fuehring¹⁵, E. Gabriel³², T. Gaintseva⁴², A. Gallas Torreira⁴⁶, D. Galli^{20,d}, S. Gambetta^{58,48},
Y. Gan³, M. Gandelman², P. Gandini²⁵, Y. Gao⁵, M. Garau²⁷, L.M. Garcia Martin⁵⁶,
P. Garcia Moreno⁴⁵, J. García Pardiñas^{26,j}, B. Garcia Plana⁴⁶, F.A. Garcia Rosales¹²,
L. Garrido⁴⁵, C. Gaspar⁴⁸, R.E. Geertsema³², D. Gerick¹⁷, L.L. Gerken¹⁵, E. Gersabeck⁶²,
M. Gersabeck⁶², T. Gershon⁵⁶, D. Gerstel¹⁰, Ph. Ghez⁸, L. Giambastiani²⁸, V. Gibson⁵⁵,
H.K. Giemza³⁶, A.L. Gilman⁶³, M. Giovannetti^{23,p}, A. Gioventù⁴⁶, P. Gironella Gironell⁴⁵,
L. Giubega³⁷, C. Giugliano^{21,f,48}, K. Gizdov⁵⁸, E.L. Gkoukousis⁴⁸, V.V. Gligorov¹³, C. Göbel⁷⁰,
E. Golobardes⁸⁵, D. Golubkov⁴¹, A. Golutvin^{61,83}, A. Gomes^{1,a}, S. Gomez Fernandez⁴⁵,
F. Goncalves Abrantes⁶³, M. Goncerz³⁵, G. Gong³, P. Gorbounov⁴¹, I.V. Gorelov⁴⁰, C. Gotti²⁶,
E. Govorkova⁴⁸, J.P. Grabowski¹⁷, T. Grammatico¹³, L.A. Granado Cardoso⁴⁸, E. Graugés⁴⁵,
E. Graverini⁴⁹, G. Graziani²², A. Grecu³⁷, L.M. Greeven³², N.A. Grieser⁴, L. Grillo⁶²,
S. Gromov⁸³, B.R. Gruberg Cazon⁶³, C. Gu³, M. Guarise²¹, P. A. Günther¹⁷, E. Gushchin³⁹,
A. Guth¹⁴, Y. Guz⁴⁴, T. Gys⁴⁸, T. Hadavizadeh⁶⁹, G. Haefeli⁴⁹, C. Haen⁴⁸, J. Haimberger⁴⁸,
T. Halewood-leagas⁶⁰, P.M. Hamilton⁶⁶, J.P. Hammerich⁶⁰, Q. Han⁷, X. Han¹⁷, T.H. Hancock⁶³,
S. Hansmann-Menzemer¹⁷, N. Harnew⁶³, T. Harrison⁶⁰, C. Hasse⁴⁸, M. Hatch⁴⁸, J. He^{6,b},
M. Hecker⁶¹, K. Heijhoff³², K. Heinicke¹⁵, A.M. Hennequin⁴⁸, K. Hennessy⁶⁰, L. Henry⁴⁸,
J. Heuel¹⁴, A. Hicheur², D. Hill⁴⁹, M. Hilton⁶², S.E. Hollitt¹⁵, R. Hou⁷, Y. Hou⁶, J. Hu¹⁷,
J. Hu⁷², W. Hu⁷, X. Hu³, W. Huang⁶, X. Huang⁷³, W. Hulsbergen³², R.J. Hunter⁵⁶,
M. Hushchyn⁸², D. Hutchcroft⁶⁰, D. Hynds³², P. Ibis¹⁵, M. Idzik³⁴, D. Ilin³⁸, P. Ilten⁶⁵,
A. Inglessi³⁸, A. Ishteev⁸³, K. Ivshin³⁸, R. Jacobsson⁴⁸, H. Jage¹⁴, S. Jakobsen⁴⁸, E. Jans³²,
B.K. Jashal⁴⁷, A. Jawahery⁶⁶, V. Jevtic¹⁵, F. Jiang³, M. John⁶³, D. Johnson⁴⁸, C.R. Jones⁵⁵,
T.P. Jones⁵⁶, B. Jost⁴⁸, N. Jurik⁴⁸, S.H. Kalavan Kadavath³⁴, S. Kandybei⁵¹, Y. Kang³,
M. Karacson⁴⁸, M. Karpov⁸², F. Keizer⁴⁸, D.M. Keller⁶⁸, M. Kenzie⁵⁶, T. Ketel³³, B. Khanji¹⁵,
A. Kharisova⁸⁴, S. Kholodenko⁴⁴, T. Kirn¹⁴, V.S. Kirsebom⁴⁹, O. Kitouni⁶⁴, S. Klaver³²,
N. Kleijne²⁹, K. Klimaszewski³⁶, M.R. Kmiec³⁶, S. Koliiev⁵², A. Kondybayeva⁸³,
A. Konoplyannikov⁴¹, P. Kopciwicz³⁴, R. Kopečna¹⁷, P. Koppenburg³², M. Korolev⁴⁰,
I. Kostiuik^{32,52}, O. Kot⁵², S. Kotriakhova^{21,38}, P. Kravchenko³⁸, L. Kravchuk³⁹,
R.D. Krawczyk⁴⁸, M. Kreps⁵⁶, F. Kress⁶¹, S. Kretzschmar¹⁴, P. Krokovny^{43,v}, W. Krupa³⁴,
W. Krzemien³⁶, W. Kucewicz^{35,t}, M. Kucharczyk³⁵, V. Kudryavtsev^{43,v}, H.S. Kuindersma^{32,33},
G.J. Kunde⁶⁷, T. Kvaratskheliya⁴¹, D. Lacarrere⁴⁸, G. Lafferty⁶², A. Lai²⁷, A. Lampis²⁷,
D. Lancierini⁵⁰, J.J. Lane⁶², R. Lane⁵⁴, G. Lanfranchi²³, C. Langenbruch¹⁴, J. Langer¹⁵,
O. Lantwin⁸³, T. Latham⁵⁶, F. Lazzari^{29,q}, R. Le Gac¹⁰, S.H. Lee⁸⁶, R. Lefèvre⁹, A. Leflat⁴⁰,
S. Legotin⁸³, O. Leroy¹⁰, T. Lesiak³⁵, B. Leverington¹⁷, H. Li⁷², P. Li¹⁷, S. Li⁷, Y. Li⁴, Y. Li⁴,
Z. Li⁶⁸, X. Liang⁶⁸, T. Lin⁶¹, R. Lindner⁴⁸, V. Lisovskyi¹⁵, R. Litvinov²⁷, G. Liu⁷², H. Liu⁶,
S. Liu⁴, A. Lobo Salvia⁴⁵, A. Loi²⁷, J. Lomba Castro⁴⁶, I. Longstaff⁵⁹, J.H. Lopes²,
S. Lopez Solino⁴⁶, G.H. Lovell⁵⁵, Y. Lu⁴, C. Lucarelli²², D. Lucchesi^{28,l}, S. Luchuk³⁹,
M. Lucio Martinez³², V. Lukashenko^{32,52}, Y. Luo³, A. Lupato⁶², E. Luppi^{21,f}, O. Lupton⁵⁶,
A. Lusiani^{29,m}, X. Lyu⁶, L. Ma⁴, R. Ma⁶, S. Maccolini^{20,d}, F. Machefer¹¹, F. Maciuc³⁷,
V. Macko⁴⁹, P. Mackowiak¹⁵, S. Maddrell-Mander⁵⁴, O. Madejczyk³⁴, L.R. Madhan Mohan⁵⁴,
O. Maev³⁸, A. Maevskiy⁸², D. Maisuzenko³⁸, M.W. Majewski³⁴, J.J. Malczewski³⁵, S. Malde⁶³,
B. Malecki⁴⁸, A. Malinin⁸¹, T. Maltsev^{43,v}, H. Malygina¹⁷, G. Manca^{27,e}, G. Mancinelli¹⁰,
D. Manuzzi^{20,d}, D. Marangotto^{25,i}, J. Maratas^{9,s}, J.F. Marchand⁸, U. Marconi²⁰, S. Mariani^{22,g},
C. Marin Benito⁴⁸, M. Marinangeli⁴⁹, J. Marks¹⁷, A.M. Marshall⁵⁴, P.J. Marshall⁶⁰,
G. Martelli⁷⁸, G. Martellotti³⁰, L. Martinazzoli^{48,j}, M. Martinelli^{26,j}, D. Martinez Santos⁴⁶,
F. Martinez Vidal⁴⁷, A. Massafferri¹, M. Materok¹⁴, R. Matev⁴⁸, A. Mathad⁵⁰, Z. Mathe⁴⁸,
V. Matiunin⁴¹, C. Matteuzzi²⁶, K.R. Mattioli⁸⁶, A. Mauri³², E. Maurice¹², J. Mauricio⁴⁵,
M. Mazurek⁴⁸, M. McCann⁶¹, L. McConnell¹⁸, T.H. Mcgrath⁶², N.T. Mchugh⁵⁹, A. McNab⁶²,
R. McNulty¹⁸, J.V. Mead⁶⁰, B. Meadows⁶⁵, G. Meier¹⁵, N. Meinert⁷⁶, D. Melnychuk³⁶,

S. Meloni^{26,j}, M. Merk^{32,80}, A. Merli^{25,i}, L. Meyer Garcia², M. Mikhasenko⁴⁸, D.A. Milanes⁷⁴,
 E. Millard⁵⁶, M. Milovanovic⁴⁸, M.-N. Minard⁸, A. Minotti^{26,j}, L. Minzoni^{21,f}, S.E. Mitchell⁵⁸,
 B. Mitreska⁶², D.S. Mitzel⁴⁸, A. Mödden¹⁵, R.A. Mohammed⁶³, R.D. Moise⁶¹,
 T. Mombächer⁴⁶, I.A. Monroy⁷⁴, S. Monteil⁹, M. Morandin²⁸, G. Morello²³, M.J. Morello^{29,m},
 J. Moron³⁴, A.B. Morris⁷⁵, A.G. Morris⁵⁶, R. Mountain⁶⁸, H. Mu³, F. Muheim^{58,48},
 M. Mulder⁴⁸, D. Müller⁴⁸, K. Müller⁵⁰, C.H. Murphy⁶³, D. Murray⁶², P. Muzzetto^{27,48},
 P. Naik⁵⁴, T. Nakada⁴⁹, R. Nandakumar⁵⁷, T. Nanut⁴⁹, I. Nasteva², M. Needham⁵⁸, I. Neri²¹,
 N. Neri^{25,i}, S. Neubert⁷⁵, N. Neufeld⁴⁸, R. Newcombe⁶¹, T.D. Nguyen⁴⁹, C. Nguyen-Mau^{49,x},
 E.M. Niel¹¹, S. Nieswand¹⁴, N. Nikitin⁴⁰, N.S. Nolte⁶⁴, C. Normand⁸, C. Nunez⁸⁶,
 A. Oblakowska-Mucha³⁴, V. Obraztsov⁴⁴, T. Oeser¹⁴, D.P. O’Hanlon⁵⁴, S. Okamura²¹,
 R. Oldeman^{27,e}, M.E. Olivares⁶⁸, C.J.G. Onderwater⁷⁹, R.H. O’Neil⁵⁸, A. Ossowska³⁵,
 J.M. Otalora Goicochea², T. Ovsianikova⁴¹, P. Owen⁵⁰, A. Oyanguren⁴⁷, K.O. Padeken⁷⁵,
 B. Pagare⁵⁶, P.R. Pais⁴⁸, T. Pajero⁶³, A. Palano¹⁹, M. Palutan²³, Y. Pan⁶², G. Panshin⁸⁴,
 A. Papanestis⁵⁷, M. Pappagallo^{19,c}, L.L. Pappalardo^{21,f}, C. Pappenheimer⁶⁵, W. Parker⁶⁶,
 C. Parkes⁶², B. Passalacqua²¹, G. Passaleva²², A. Pastore¹⁹, M. Patel⁶¹, C. Patrignani^{20,d},
 C.J. Pawley⁸⁰, A. Pearce⁴⁸, A. Pellegrino³², M. Pepe Altarelli⁴⁸, S. Perazzini²⁰, D. Pereima⁴¹,
 A. Pereiro Castro⁴⁶, P. Perret⁹, M. Petric^{59,48}, K. Petridis⁵⁴, A. Petrolini^{24,h}, A. Petrov⁸¹,
 S. Petrucci⁵⁸, M. Petruzzo²⁵, T.T.H. Pham⁶⁸, A. Philippov⁴², L. Pica^{29,m}, M. Piccini⁷⁸,
 B. Pietrzyk⁸, G. Pietrzyk⁴⁹, M. Pili⁶³, D. Pinci³⁰, F. Pisani⁴⁸, M. Pizzichemi^{26,48,j}, Resmi
 P.K¹⁰, V. Placinta³⁷, J. Plews⁵³, M. Plo Casasus⁴⁶, F. Polci¹³, M. Poli Lener²³, M. Poliakov⁶⁸,
 A. Poluektov¹⁰, N. Polukhina^{83,u}, I. Polyakov⁶⁸, E. Polycarpo², S. Ponce⁴⁸, D. Popov^{6,48},
 S. Popov⁴², S. Poslavskii⁴⁴, K. Prasanth³⁵, L. Promberger⁴⁸, C. Prouve⁴⁶, V. Pugatch⁵²,
 V. Puill¹¹, H. Pullen⁶³, G. Punzi^{29,n}, H. Qi³, W. Qian⁶, J. Qin⁶, N. Qin³, R. Quagliani¹³,
 B. Quintana⁸, N.V. Raab¹⁸, R.I. Rabadan Trejo⁶, B. Rachwal³⁴, J.H. Rademacker⁵⁴,
 M. Rama²⁹, M. Ramos Pernas⁵⁶, M.S. Rangel², F. Ratnikov^{42,82}, G. Raven³³, M. Reboud⁸,
 F. Redi⁴⁹, F. Reiss⁶², C. Remon Alepuz⁴⁷, Z. Ren³, V. Renaudin⁶³, R. Ribatti²⁹, S. Ricciardi⁵⁷,
 K. Rinnert⁶⁰, P. Robbe¹¹, G. Robertson⁵⁸, A.B. Rodrigues⁴⁹, E. Rodrigues⁶⁰,
 J.A. Rodriguez Lopez⁷⁴, E.R.R. Rodriguez Rodriguez⁴⁶, A. Rollings⁶³, P. Roloff⁴⁸,
 V. Romanovskiy⁴⁴, M. Romero Lamas⁴⁶, A. Romero Vidal⁴⁶, J.D. Roth⁸⁶, M. Rotondo²³,
 M.S. Rudolph⁶⁸, T. Ruf⁴⁸, R.A. Ruiz Fernandez⁴⁶, J. Ruiz Vidal⁴⁷, A. Ryzhikov⁸², J. Ryzka³⁴,
 J.J. Saborido Silva⁴⁶, N. Sagidova³⁸, N. Sahoo⁵⁶, B. Saitta^{27,e}, M. Salomoni⁴⁸,
 C. Sanchez Gras³², R. Santacesaria³⁰, C. Santamarina Rios⁴⁶, M. Santimaria²³,
 E. Santovetti^{31,p}, D. Saranin⁸³, G. Sarpis¹⁴, M. Sarpis⁷⁵, A. Sarti³⁰, C. Satriano^{30,o}, A. Satta³¹,
 M. Saur¹⁵, D. Savrina^{41,40}, H. Sazak⁹, L.G. Scantlebury Smead⁶³, A. Scarabotto¹³, S. Schael¹⁴,
 S. Scherl⁶⁰, M. Schiller⁵⁹, H. Schindler⁴⁸, M. Schmelling¹⁶, B. Schmidt⁴⁸, S. Schmitt¹⁴,
 O. Schneider⁴⁹, A. Schopper⁴⁸, M. Schubiger³², S. Schulte⁴⁹, M.H. Schune¹¹, R. Schwemmer⁴⁸,
 B. Sciascia²³, S. Sellam⁴⁶, A. Semennikov⁴¹, M. Senghi Soares³³, A. Sergi^{24,h}, N. Serra⁵⁰,
 L. Sestini²⁸, A. Seuthe¹⁵, Y. Shang⁵, D.M. Shangase⁸⁶, M. Shapkin⁴⁴, I. Shchemerov⁸³,
 L. Shchutska⁴⁹, T. Shears⁶⁰, L. Shekhtman^{43,v}, Z. Shen⁵, V. Shevchenko⁸¹, E.B. Shields^{26,j},
 Y. Shimizu¹¹, E. Shmanin⁸³, J.D. Shupperd⁶⁸, B.G. Siddi²¹, R. Silva Coutinho⁵⁰, G. Simi²⁸,
 S. Simone^{19,c}, N. Skidmore⁶², T. Skwarnicki⁶⁸, M.W. Slater⁵³, I. Slazyk^{21,f}, J.C. Smallwood⁶³,
 J.G. Smeaton⁵⁵, A. Smetkina⁴¹, E. Smith⁵⁰, M. Smith⁶¹, A. Snoch³², M. Soares²⁰,
 L. Soares Lavra⁹, M.D. Sokoloff⁶⁵, F.J.P. Soler⁵⁹, A. Solovev³⁸, I. Solovyev³⁸,
 F.L. Souza De Almeida², B. Souza De Paula², B. Spaan¹⁵, E. Spadaro Norella^{25,i}, P. Spradlin⁵⁹,
 F. Stagni⁴⁸, M. Stahl⁶⁵, S. Stahl⁴⁸, S. Stanislaus⁶³, O. Steinkamp^{50,83}, O. Stenyakin⁴⁴,
 H. Stevens¹⁵, S. Stone⁶⁸, M.E. Stramaglia⁴⁹, M. Straticiu³⁷, D. Strelakina⁸³, F. Suljik⁶³,
 J. Sun²⁷, L. Sun⁷³, Y. Sun⁶⁶, P. Svihra⁶², P.N. Swallow⁵³, K. Swientek³⁴, A. Szabelski³⁶,
 T. Szumlak³⁴, M. Szymanski⁴⁸, S. Taneja⁶², A.R. Tanner⁵⁴, M.D. Tat⁶³, A. Terentev⁸³,
 F. Teubert⁴⁸, E. Thomas⁴⁸, D.J.D. Thompson⁵³, K.A. Thomson⁶⁰, V. Tisserand⁹,
 S. T’Jampens⁸, M. Tobin⁴, L. Tomassetti^{21,f}, X. Tong⁵, D. Torres Machado¹, D.Y. Tou¹³,

M.T. Tran⁴⁹, E. Trifonova⁸³, C. Trippel⁴⁹, G. Tuci^{29,n}, A. Tully⁴⁹, N. Tuning^{32,48}, A. Ukleja³⁶, D.J. Unverzagt¹⁷, E. Ursov⁸³, A. Usachov³², A. Ustyuzhanin^{42,82}, U. Uwer¹⁷, A. Vagner⁸⁴, V. Vagnoni²⁰, A. Valassi⁴⁸, G. Valenti²⁰, N. Valls Canudas⁸⁵, M. van Beuzekom³², M. Van Dijk⁴⁹, E. van Herwijnen⁸³, C.B. Van Hulse¹⁸, M. van Veghel⁷⁹, R. Vazquez Gomez⁴⁵, P. Vazquez Regueiro⁴⁶, C. Vázquez Sierra⁴⁸, S. Vecchi²¹, J.J. Velthuis⁵⁴, M. Veltri^{22,r}, A. Venkateswaran⁶⁸, M. Veronesi³², M. Vesterinen⁵⁶, D. Vieira⁶⁵, M. Vieites Diaz⁴⁹, H. Viemann⁷⁶, X. Vilasis-Cardona⁸⁵, E. Vilella Figueras⁶⁰, A. Villa²⁰, P. Vincent¹³, F.C. Volle¹¹, D. Vom Bruch¹⁰, A. Vorobyev³⁸, V. Vorobyev^{43,v}, N. Voropaev³⁸, K. Vos⁸⁰, R. Waldi¹⁷, J. Walsh²⁹, C. Wang¹⁷, J. Wang⁵, J. Wang⁴, J. Wang³, J. Wang⁷³, M. Wang³, R. Wang⁵⁴, Y. Wang⁷, Z. Wang⁵⁰, Z. Wang³, Z. Wang⁶, J.A. Ward⁵⁶, H.M. Wark⁶⁰, N.K. Watson⁵³, S.G. Weber¹³, D. Websdale⁶¹, C. Weisser⁶⁴, B.D.C. Westhenry⁵⁴, D.J. White⁶², M. Whitehead⁵⁴, A.R. Wiederhold⁵⁶, D. Wiedner¹⁵, G. Wilkinson⁶³, M. Wilkinson⁶⁸, I. Williams⁵⁵, M. Williams⁶⁴, M.R.J. Williams⁵⁸, F.F. Wilson⁵⁷, W. Wislicki³⁶, M. Witek³⁵, L. Witola¹⁷, G. Wormser¹¹, S.A. Wotton⁵⁵, H. Wu⁶⁸, K. Wyllie⁴⁸, Z. Xiang⁶, D. Xiao⁷, Y. Xie⁷, A. Xu⁵, J. Xu⁶, L. Xu³, M. Xu⁷, Q. Xu⁶, Z. Xu⁵, Z. Xu⁶, D. Yang³, S. Yang⁶, Y. Yang⁶, Z. Yang⁵, Z. Yang⁶⁶, Y. Yao⁶⁸, L.E. Yeomans⁶⁰, H. Yin⁷, J. Yu⁷¹, X. Yuan⁶⁸, O. Yushchenko⁴⁴, E. Zaffaroni⁴⁹, M. Zavertyaev^{16,u}, M. Zdybal³⁵, O. Zenaiev⁴⁸, M. Zeng³, D. Zhang⁷, L. Zhang³, S. Zhang⁷¹, S. Zhang⁵, Y. Zhang⁵, Y. Zhang⁶³, A. Zharkova⁸³, A. Zhelezov¹⁷, Y. Zheng⁶, T. Zhou⁵, X. Zhou⁶, Y. Zhou⁶, V. Zhovkovska¹¹, X. Zhu³, X. Zhu⁷, Z. Zhu⁶, V. Zhukov^{14,40}, J.B. Zonneveld⁵⁸, Q. Zou⁴, S. Zucchelli^{20,d}, D. Zuliani²⁸, G. Zunica⁶².

¹Centro Brasileiro de Pesquisas Físicas (CBPF), Rio de Janeiro, Brazil

²Universidade Federal do Rio de Janeiro (UFRJ), Rio de Janeiro, Brazil

³Center for High Energy Physics, Tsinghua University, Beijing, China

⁴Institute Of High Energy Physics (IHEP), Beijing, China

⁵School of Physics State Key Laboratory of Nuclear Physics and Technology, Peking University, Beijing, China

⁶University of Chinese Academy of Sciences, Beijing, China

⁷Institute of Particle Physics, Central China Normal University, Wuhan, Hubei, China

⁸Univ. Savoie Mont Blanc, CNRS, IN2P3-LAPP, Annecy, France

⁹Université Clermont Auvergne, CNRS/IN2P3, LPC, Clermont-Ferrand, France

¹⁰Aix Marseille Univ, CNRS/IN2P3, CPPM, Marseille, France

¹¹Université Paris-Saclay, CNRS/IN2P3, IJCLab, Orsay, France

¹²Laboratoire Leprince-Ringuet, CNRS/IN2P3, Ecole Polytechnique, Institut Polytechnique de Paris, Palaiseau, France

¹³LPNHE, Sorbonne Université, Paris Diderot Sorbonne Paris Cité, CNRS/IN2P3, Paris, France

¹⁴I. Physikalisches Institut, RWTH Aachen University, Aachen, Germany

¹⁵Fakultät Physik, Technische Universität Dortmund, Dortmund, Germany

¹⁶Max-Planck-Institut für Kernphysik (MPIK), Heidelberg, Germany

¹⁷Physikalisches Institut, Ruprecht-Karls-Universität Heidelberg, Heidelberg, Germany

¹⁸School of Physics, University College Dublin, Dublin, Ireland

¹⁹INFN Sezione di Bari, Bari, Italy

²⁰INFN Sezione di Bologna, Bologna, Italy

²¹INFN Sezione di Ferrara, Ferrara, Italy

²²INFN Sezione di Firenze, Firenze, Italy

²³INFN Laboratori Nazionali di Frascati, Frascati, Italy

²⁴INFN Sezione di Genova, Genova, Italy

²⁵INFN Sezione di Milano, Milano, Italy

²⁶INFN Sezione di Milano-Bicocca, Milano, Italy

²⁷INFN Sezione di Cagliari, Monserrato, Italy

²⁸Università degli Studi di Padova, Università e INFN, Padova, Padova, Italy

²⁹INFN Sezione di Pisa, Pisa, Italy

³⁰INFN Sezione di Roma La Sapienza, Roma, Italy

³¹INFN Sezione di Roma Tor Vergata, Roma, Italy

- ³² *Nikhef National Institute for Subatomic Physics, Amsterdam, Netherlands*
- ³³ *Nikhef National Institute for Subatomic Physics and VU University Amsterdam, Amsterdam, Netherlands*
- ³⁴ *AGH - University of Science and Technology, Faculty of Physics and Applied Computer Science, Kraków, Poland*
- ³⁵ *Henryk Niewodniczanski Institute of Nuclear Physics Polish Academy of Sciences, Kraków, Poland*
- ³⁶ *National Center for Nuclear Research (NCBJ), Warsaw, Poland*
- ³⁷ *Horia Hulubei National Institute of Physics and Nuclear Engineering, Bucharest-Magurele, Romania*
- ³⁸ *Petersburg Nuclear Physics Institute NRC Kurchatov Institute (PNPI NRC KI), Gatchina, Russia*
- ³⁹ *Institute for Nuclear Research of the Russian Academy of Sciences (INR RAS), Moscow, Russia*
- ⁴⁰ *Institute of Nuclear Physics, Moscow State University (SINP MSU), Moscow, Russia*
- ⁴¹ *Institute of Theoretical and Experimental Physics NRC Kurchatov Institute (ITEP NRC KI), Moscow, Russia*
- ⁴² *Yandex School of Data Analysis, Moscow, Russia*
- ⁴³ *Budker Institute of Nuclear Physics (SB RAS), Novosibirsk, Russia*
- ⁴⁴ *Institute for High Energy Physics NRC Kurchatov Institute (IHEP NRC KI), Protvino, Russia, Protvino, Russia*
- ⁴⁵ *ICCUB, Universitat de Barcelona, Barcelona, Spain*
- ⁴⁶ *Instituto Galego de Física de Altas Enerxías (IGFAE), Universidade de Santiago de Compostela, Santiago de Compostela, Spain*
- ⁴⁷ *Instituto de Física Corpuscular, Centro Mixto Universidad de Valencia - CSIC, Valencia, Spain*
- ⁴⁸ *European Organization for Nuclear Research (CERN), Geneva, Switzerland*
- ⁴⁹ *Institute of Physics, Ecole Polytechnique Fédérale de Lausanne (EPFL), Lausanne, Switzerland*
- ⁵⁰ *Physik-Institut, Universität Zürich, Zürich, Switzerland*
- ⁵¹ *NSC Kharkiv Institute of Physics and Technology (NSC KIPT), Kharkiv, Ukraine*
- ⁵² *Institute for Nuclear Research of the National Academy of Sciences (KINR), Kyiv, Ukraine*
- ⁵³ *University of Birmingham, Birmingham, United Kingdom*
- ⁵⁴ *H.H. Wills Physics Laboratory, University of Bristol, Bristol, United Kingdom*
- ⁵⁵ *Cavendish Laboratory, University of Cambridge, Cambridge, United Kingdom*
- ⁵⁶ *Department of Physics, University of Warwick, Coventry, United Kingdom*
- ⁵⁷ *STFC Rutherford Appleton Laboratory, Didcot, United Kingdom*
- ⁵⁸ *School of Physics and Astronomy, University of Edinburgh, Edinburgh, United Kingdom*
- ⁵⁹ *School of Physics and Astronomy, University of Glasgow, Glasgow, United Kingdom*
- ⁶⁰ *Oliver Lodge Laboratory, University of Liverpool, Liverpool, United Kingdom*
- ⁶¹ *Imperial College London, London, United Kingdom*
- ⁶² *Department of Physics and Astronomy, University of Manchester, Manchester, United Kingdom*
- ⁶³ *Department of Physics, University of Oxford, Oxford, United Kingdom*
- ⁶⁴ *Massachusetts Institute of Technology, Cambridge, MA, United States*
- ⁶⁵ *University of Cincinnati, Cincinnati, OH, United States*
- ⁶⁶ *University of Maryland, College Park, MD, United States*
- ⁶⁷ *Los Alamos National Laboratory (LANL), Los Alamos, United States*
- ⁶⁸ *Syracuse University, Syracuse, NY, United States*
- ⁶⁹ *School of Physics and Astronomy, Monash University, Melbourne, Australia, associated to ⁵⁶*
- ⁷⁰ *Pontifícia Universidade Católica do Rio de Janeiro (PUC-Rio), Rio de Janeiro, Brazil, associated to ²*
- ⁷¹ *Physics and Micro Electronic College, Hunan University, Changsha City, China, associated to ⁷*
- ⁷² *Guangdong Provincial Key Laboratory of Nuclear Science, Guangdong-Hong Kong Joint Laboratory of Quantum Matter, Institute of Quantum Matter, South China Normal University, Guangzhou, China, associated to ³*
- ⁷³ *School of Physics and Technology, Wuhan University, Wuhan, China, associated to ³*
- ⁷⁴ *Departamento de Física, Universidad Nacional de Colombia, Bogota, Colombia, associated to ¹³*
- ⁷⁵ *Universität Bonn - Helmholtz-Institut für Strahlen und Kernphysik, Bonn, Germany, associated to ¹⁷*
- ⁷⁶ *Institut für Physik, Universität Rostock, Rostock, Germany, associated to ¹⁷*
- ⁷⁷ *Eotvos Lorand University, Budapest, Hungary, associated to ⁴⁸*
- ⁷⁸ *INFN Sezione di Perugia, Perugia, Italy, associated to ²¹*
- ⁷⁹ *Van Swinderen Institute, University of Groningen, Groningen, Netherlands, associated to ³²*
- ⁸⁰ *Universiteit Maastricht, Maastricht, Netherlands, associated to ³²*

- ⁸¹ *National Research Centre Kurchatov Institute, Moscow, Russia, associated to* ⁴¹
- ⁸² *National Research University Higher School of Economics, Moscow, Russia, associated to* ⁴²
- ⁸³ *National University of Science and Technology "MISIS", Moscow, Russia, associated to* ⁴¹
- ⁸⁴ *National Research Tomsk Polytechnic University, Tomsk, Russia, associated to* ⁴¹
- ⁸⁵ *DS4DS, La Salle, Universitat Ramon Llull, Barcelona, Spain, associated to* ⁴⁵
- ⁸⁶ *University of Michigan, Ann Arbor, United States, associated to* ⁶⁸
- ^a *Universidade Federal do Triângulo Mineiro (UFTM), Uberaba-MG, Brazil*
- ^b *Hangzhou Institute for Advanced Study, UCAS, Hangzhou, China*
- ^c *Università di Bari, Bari, Italy*
- ^d *Università di Bologna, Bologna, Italy*
- ^e *Università di Cagliari, Cagliari, Italy*
- ^f *Università di Ferrara, Ferrara, Italy*
- ^g *Università di Firenze, Firenze, Italy*
- ^h *Università di Genova, Genova, Italy*
- ⁱ *Università degli Studi di Milano, Milano, Italy*
- ^j *Università di Milano Bicocca, Milano, Italy*
- ^k *Università di Modena e Reggio Emilia, Modena, Italy*
- ^l *Università di Padova, Padova, Italy*
- ^m *Scuola Normale Superiore, Pisa, Italy*
- ⁿ *Università di Pisa, Pisa, Italy*
- ^o *Università della Basilicata, Potenza, Italy*
- ^p *Università di Roma Tor Vergata, Roma, Italy*
- ^q *Università di Siena, Siena, Italy*
- ^r *Università di Urbino, Urbino, Italy*
- ^s *MSU - Iligan Institute of Technology (MSU-IIT), Iligan, Philippines*
- ^t *AGH - University of Science and Technology, Faculty of Computer Science, Electronics and Telecommunications, Kraków, Poland*
- ^u *P.N. Lebedev Physical Institute, Russian Academy of Science (LPI RAS), Moscow, Russia*
- ^v *Novosibirsk State University, Novosibirsk, Russia*
- ^w *Department of Physics and Astronomy, Uppsala University, Uppsala, Sweden*
- ^x *Hanoi University of Science, Hanoi, Vietnam*